ACS APPLIED MATERIALS & INTERFACES

Research Article

www.acsami.org

Thermal Treatment Effects on Charge Storage Performance of Graphene-Based Materials for Supercapacitors

Hongxin Zhang, Vinay V. Bhat, Nidia C. Gallego, and Cristian I. Contescu*

Materials Science and Technology Division, Oak Ridge National Laboratory, P.O. Box 2008, MS-6087, Oak Ridge, Tennessee 37831, United States

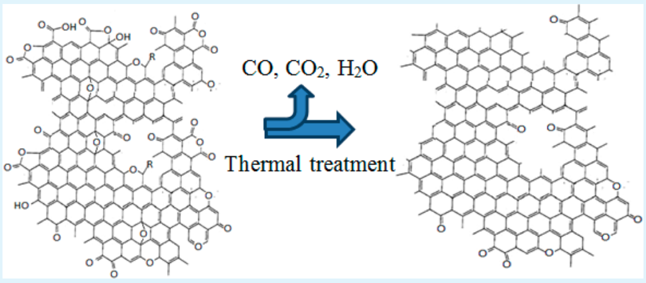

ABSTRACT: Graphene materials were synthesized by reduction of exfoliated graphite oxide and then thermally treated in nitrogen to improve the surface area and their electrochemical performance as electrical double-layer capacitor electrodes. The structural and surface properties of the prepared reduced graphite oxide (RGO) were investigated using atomic force microscopy, scanning electron microscopy, Raman spectra, X-ray diffraction pattern analysis, and nitrogen adsorption/desorption studies. RGO forms a continuous network of crumpled sheets, which consist of large amounts of few-layer and single-layer graphenes. Electrochemical studies were conducted by cyclic voltammetry, impedance spectroscopy, and galvanostatic charge−discharge measurements. The modified RGO materials showed enhanced electrochemical performance, with maximum specific capacitance of 96 F/g, energy density of 12.8 Wh/kg, and power density of 160 kW/kg. These results demonstrate that thermal treatment of RGO at selected conditions is a convenient and efficient method for improving its specific capacitance, energy, and power density.

KEYWORDS: *graphene-based materials, supercapacitor, thermal treatment, surface modification*

1. INTRODUCTION

To meet the increasing energy demands while reducing the environment impact, low cost, environmentally friendly, and more efficient energy storage devices with high charge and discharge rate are essentially needed.[1,2] Electrochemical capacitors, also called supercapacitors, storing energy by ion adsorption on conductive electrodes with large surface area, bridge the gap between conventional electrolytic capacitors and batteries.[3,4] Supercapacitors are not limited by electrochemical charge transfer kinetics, they have very long lifetimes (more than a million cycles) and can operate at high charge and discharge rates.[3,4] However, the applications of supercapacitors are still limited in industry because of the low stored energy when compared with batteries.[4,5]

Supercapacitors use reversible adsorption of electrolyte ions onto high specific surface area materials to electrostatically store the charge. Thus, increasing the efficiency of electrolyte ions adsorption is one of the keys to generate high specific capacitance. So far, different materials, such as carbon materials from various sources,[6,7] mixed metal oxides,[8] and conducting polymers[9,10] have been investigated for supercapacitor applications. Along with development of new materials, the progress in understanding charge storage mechanisms[11,12] resulted in notable performance improvements. Among the key factors that dictate selection of electrode materials, the need for high specific surface area ranks first, followed by good wettability, and fast transport of electrolyte ions through interconnected pores.[13] Carbon nanotubes (CNTs) demonstrate good capacitive performance due to the high electrical conductance.[14] Furthermore, the use of carbon nanotubes enable adaptable and flexible devices, and further advanced microelectrochemical capacitors. However, the synthesis of low-cost and high-quality SWNTs is still a huge hurdle for commercialization on CNT-based supercapacitor.[4]

Graphene emerges as a potential supercapacitor material due to its large surface area (theoretically 2630 m^2/g), very high electrical (~104 Ω^{-1} cm^{-1}) and thermal conductivity (~5000 W/(m·K)).[15,16] The large surface area can help to store more charges at the electrode−electrolyte interface. The high conductivity enables easy transport of electrons from the electrode to the current collector with little resistive energy loss, which improves the power of the device. This motivates a continuously growing interest in graphene materials for supercapacitor applications.[17,18] Graphene materials were synthesized and isolated by reducing graphite oxide using a solution-based chemical process.[19] Ruoff and co-workers[17] used the reduced graphene materials for supercapacitor application, and demonstrated that graphenes can store nearly equal amount of energy as that of commercially used activated carbons, even though their surface area was much lower than that of the latter (1500 m^2/g). This finding suggests the opportunity to further enhance the energy storage capacity of graphene materials by optimizing the synthesis conditions and eventually increasing the surface area. Wang et al. demonstrated

Received: April 5, 2012
Accepted: June 9, 2012
Published: June 10, 2012

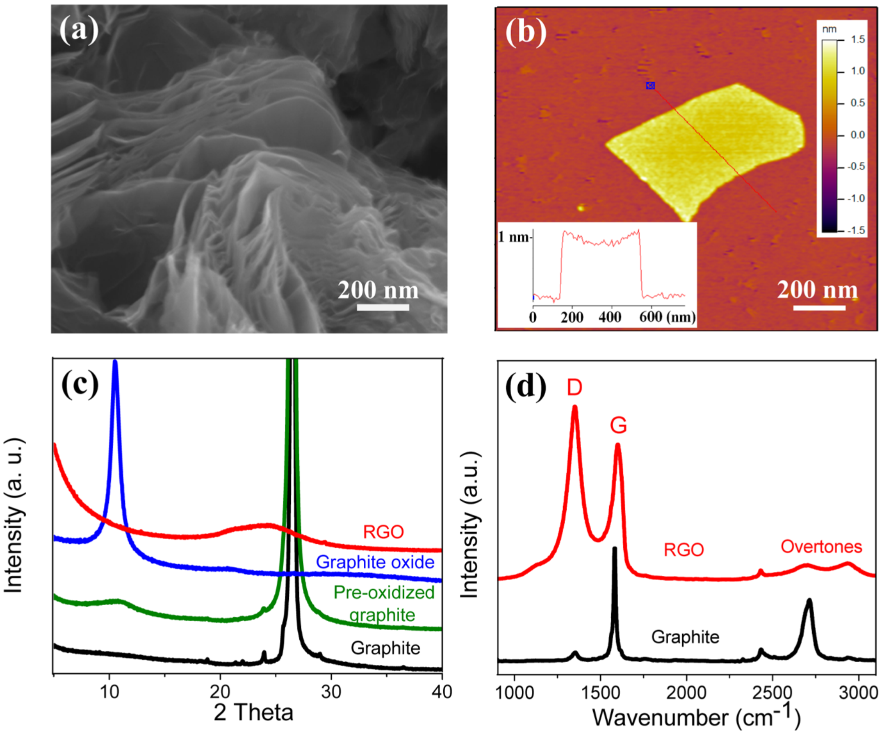

Figure 1. (a) SEM image of obtained RGO materials; (b) AFM image of RGO and height profile plot (inset) showing ~1 nm thickness of RGO sheets. (c) XRD spectra of the original graphite, preoxidized graphite, graphite oxide and RGO materials. (d) Raman spectra of graphite and RGO show typical D and G bands. The intensity ratio $I_D/I_G > 1$ indicates the presence of defects and disorder in the carbon structure.

that slight modification of synthesis conditions can nearly double the energy storage capacity of graphenes (~180 F/g).[20] They also showed that these materials can have long cycle life without any significant capacity loss. Very recently, Ruoff's team reported the synthesis of a porous carbon (BET surface area about 3100 m^2/g) using chemical activation of exfoliated graphite oxide. Gravimetric capacitance ~166 F/g was obtained from supercapacitors constructed with this carbon and the maximum energy density was 70 Wh/kg in ionic liguid.[18] To further improve the energy storage capacity of graphene materials, there are two possibilities: either optimize the synthesis conditions to prepare large surface area graphenes, or modify the morphology and surface chemistry of graphenes. Both of these approaches are mutually complementing. However, the mechanism of surface modification of graphene materials and its effects on nanostructure, pore development, and electrochemical performance has not been sufficiently investigated. Zhao et al reported on supercapacitor performance of Reduced Graphite Oxide (RGO) with different reduction levels produced through thermal reduction of graphite oxide.[21] They found that the variation of oxygen-containing groups was the main factor that affected the capacitor performance for graphene reduced by the pyrolytic method, but they have not investigated the effect on hydrazine-reduced graphenes.

In our work, we studied the effect of thermal treatment on structures, surface area, pore development and electrochemical performance of RGO materials reduced by hydrazine. Modified RGO materials showed enhanced electrochemical performance. We demonstrate that thermal treatment at selected conditions is a convenient and efficient method for improving RGO's specific capacitance, energy, and power density.

2. EXPERIMENTAL SECTION

2.1. Graphene Materials Synthesis and Modification.

Graphene materials were synthesized by a colloidal chemistry method based on oxidation and exfoliation of graphite, followed by liquid phase reduction of graphite oxide. Initially, the modified Hummers method was used to oxidize the graphite powders,[22] which involves two stages of oxidation, using first $K_2S_2O_8$ and P_2O_5 in acidic medium (H_2SO_4), and later a strong oxidizing mixture (H_2SO_4 and $KMnO_4$) for total oxidation. Graphene oxide is easily dispersible in water, but has relatively low conductivity due to the damage of the graphene network during preparation process and cannot be used directly in supercapacitors. Hence, the prepared graphite oxide materials were separated and reduced using hydrazine to restore graphene structure and conductivity, while maintaining the maximum dispersion level possible of graphene sheets. About 10 g graphite oxide was sonicated with 500 mL of DI water in a round-bottom flask. Then, 10 mL of hydrazine hydrate (32.2 mmol, Acros Organics) was added, and the flask was placed in an oil bath where the temperature was kept at 100 °C for 24 h. The precipitated black solid product was isolated, washed with copious amounts of DI water, and dried at 110 °C. This method produces a large amount of single and multilayered graphene material.

Reduced graphite oxide (RGO) still contains numerous oxygen-containing functional groups, identified as in-plane epoxide bridges, interplane peroxide-like linkages,[23] and carboxyl groups at edge carbon sites.[24] These groups are unwanted for electrochemical charge storage, and can be removed by thermal treatment in inert gas. In this study, RGO was placed in a quartz tube furnace and heated in nitrogen at 200, 400, 600, and 800 °C, respectively under a continuous flow of nitrogen (3 L/min). The heating rate was 5 °C/min and the duration was 30 min at each temperature. After the thermal treatment, the samples were cooled in the tube furnace still under flowing nitrogen, then transferred, and sealed in glass vials. Before BET measurement, each sample was outgassed under vacuum for 2 h at 300 °C to remove the gas adsorbed during the transfer process. Thermally treated samples were labeled RGO-X, where X denoted the treatment temperature.

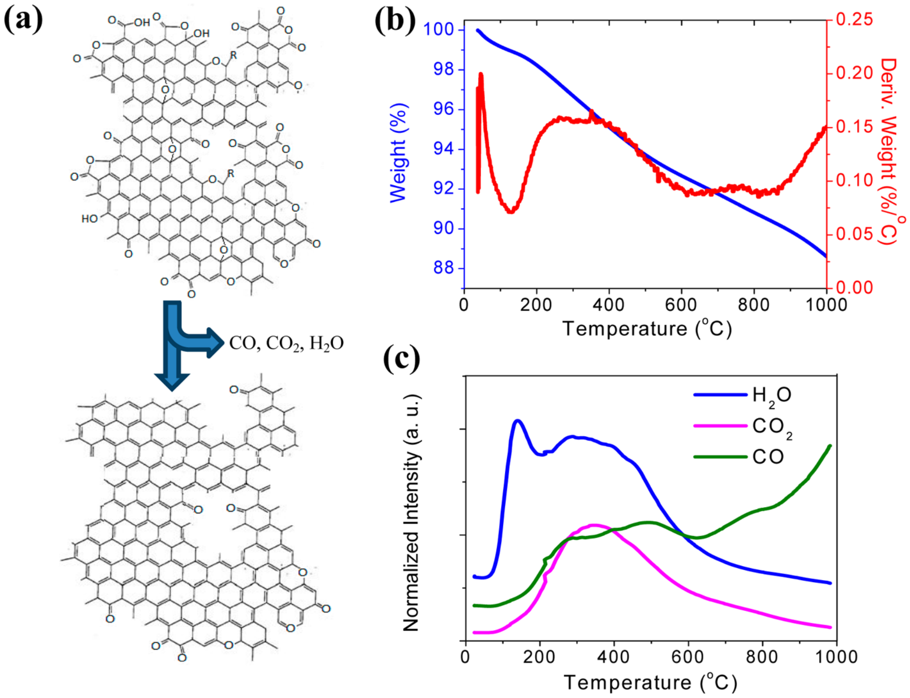

Figure 2. (a) Schematic representing selective removal of oxygen-containing functional groups through thermal treatment and release of CO, CO_2, and H_2O. (b) TGA analysis simulating the modification of RGO materials: the weight loss and the derivative weight loss versus temperature. (c) Variation in CO, CO_2, and H_2O mass spectra signals during TPD analysis from room temperature up to 1000 °C. Equal heating rate (10 °C/min) was used in both TGA and TPD measurements.

2.2. Characterization. The morphology of all samples was characterized using atomic force microscopy (AFM) and scanning electron microscopy (SEM). X-ray diffraction (XRD) pattern analysis was performed on a Philips X'Pert Pro MPD X-ray diffractometer using Ni-filtered Cu Kα radiation (λ = 1.5418 Å). Raman scattering spectra were obtained at room temperature with an excitation wavelength of 514 nm (Ar^+ ion laser).

RGO was subjected to thermogravimetric analysis (TGA) in nitrogen atmosphere at heating rate of 10 °C/min using the Q5000 TGA machine from TA Instruments. In parallel experiments, the heat treatment at 10 °C/min was replicated in temperature-programmed desorption (TPD) experiments using the Autosorb 1C instrument (Quantachrome Corporation) coupled with a quadrupole mass spectrometer (Prisma QME-200 from Pfeiffer Vacuum). The carrier gas in these experiments was helium. N_2 adsorption−desorption were measured by Autosorb 1C instrument at 77 K to investigate the surface area and pore structures of RGO. The BET surface area[25] was calculated from N_2 adsorption data at relative pressures from 0.05 to 0.3. Pore size distribution was calculated from N_2 data by the Quantachrome commercial software using the nonlocal density functional theory (NLDFT) method.[26]

2.3. Fabrication of Supercapacitor Electrodes. The capacitors for electrochemical tests were fabricated by pressing two 1 cm^2 titanium foil electrodes (~0.25 mm thick, 99.9% metal basis from Sigma-Aldrich), each carrying a thin layer of graphene material which was carefully weighed (total 3.0 − 3.5 mg) in dry state. A filter paper saturated with 5 M H_2SO_4 was sandwiched between the two electrodes, and a constant pressure was applied by using an insulated metal vice. The counter and working connectors to the electrochemical station were attached directly to each electrode.

2.4. Measurements of Electrochemical Properties. The electrochemical properties were investigated by galvanostatic charge−discharge measurements, cyclic voltammetry (CV), and electrochemical impedance spectroscopy (EIS) using a Gamry Reference 600 Potentiostat/Galvanostat/ZRA (Gamry Instruments, Inc.). The CV response of the two electrodes was recorded at scan rates between 5 and 50 mV/s. Galvanostatic charge−discharge tests were carried out over 1 V potential window at 1, 3, and 5 mA constant current. EIS measurements were carried out from 1 MHz to 10 mHz at a dc bias of 1 V and sinusoidal signal of 5 mV.

3. RESULTS AND DISCUSSION

The SEM image of the RGO materials is shown in Figure 1a. The RGO sheets exist as aggregated and crumpled layers closely associated with each other, in a continuous network. In this structure, the electrolyte ions should have great access to the inner and outer regions of the solid material, compared with the conventional activated carbon powders used in commercial capacitors. In an ideal situation, both sides of RGO sheets exposed to the electrolyte contribute to higher capacitance. The AFM image in Figure 1b and the corresponding height profile shows a 1.1 nm thick platelet, which is close to the thickness of monolayer corrugated graphenes[27] and single-layer graphite oxide rich in epoxy linkages and physisorbed water molecules held on both sides.

Figure 1c shows the XRD patterns for the original graphite, graphite preoxidized in stage I (with H_2SO_4 $K_2S_2O_8$, and P_2O_5), graphite oxide after stage II oxidation (with H_2SO_4 and $KMnO_4$), and for the final RGO material. The sharp (002) diffraction line of the graphite at 26.2° shows an interlayer distance of 3.36 ± 0.005 Å. As oxidation proceeded, the intensity of the (002) peak gradually weakened and finally disappeared. Simultaneously, the intensity of a new diffraction peak at 10.5° increased with oxidation, showing the progress of intercalation and exfoliation of the original graphite. Similar results were reported.[28,29] In the fully oxidized graphite, the (002) diffraction line disappeared almost completely and the interlayer distance of the graphite oxide increased to 8.44 ± 0.005 Å. After hydrazine reduction of graphite oxide, the peak at 10.5° completely disappeared, and a broad peak located at around 24° was found, showing that the structure of stacked

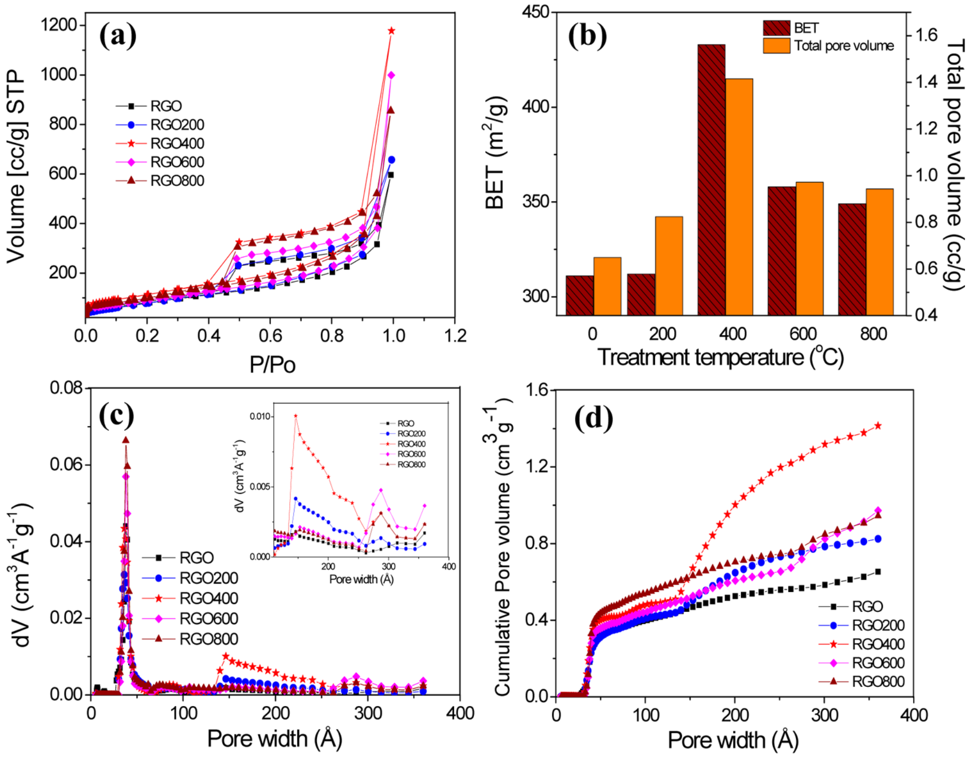

Figure 3. Gas adsorption/desorption analysis: (a) N_2 (77 K) adsorption/desorption isotherms of RGO materials thermally treated at different temperatures; (b) effect of thermal treatment on BET surface area and total pore volume; (c) differential pore size distributions from N_2 adsorption isotherms; (d) cumulative pore size distributions calculated by the NLDFT method. Microporosity (<20 Å) is absent and all pores are in the mesopore range (20−500 Å).

graphene sheets re-emerged. The broad XRD peak of the RGO samples suggests high stacking disorder in the through-plane direction of the RGO samples, small size of coherently stacked graphenes, and other structural defects.

The structural changes occurring during the chemical processing from pristine graphite to RGO are also reflected in their Raman spectra shown in Figure 1d. The typical features for carbon in Raman spectra are the D line around 1350 cm^{-1}, which is usually assigned to the E_{2g} phonon of C sp^2 atoms, and the G line around 1582 cm^{-1}, which is a breathing mode of κ-point phonons of A_{1g} symmetry.[30] The overtone of the D line, the D′ line, is located at 2700 cm^{-1}, whereas the G′ line (the overtone of the G line) is around 3248 cm^{-1}.[19] The Raman spectrum of the pristine natural graphite in Figure 1d displays a strong G peak at 1582 cm^{-1}, a weak D line at 1350 cm^{-1} and a broad D′ line at 2690 cm^{-1}. In the Raman spectrum of RGO material, the broadened G band shifted to 1595 cm^{-1}. These changes are attributed to the significant decrease of the size of in-plane sp^2 domains due to oxidation, and the presence of partially ordered graphite-like structures in RGO.[29] Meanwhile, the intensity of the D band at 1350 cm^{-1} increases substantially, showing the presence of defects and disorder in the carbon structure.

Oxygen-containing functional groups still exist on the surface of RGO materials after reduction with hydrazine. The major oxygen functional groups on oxidized carbons[31,32] and graphite[33] are anhydride, carboxyl, phenol, lactone, quinone, and carbonyl groups. Some functional groups (epoxy bridges and peroxide linkages) were confirmed even after reduction of graphene oxides.[23] These oxygen-containing functional groups improve the electrode wettability and thus enhance the overall capacitor performance.[34] However, not all these groups are useful for reversible electrochemical redox reactions. Specifically, redox reactions between quinone and phenol groups contribute additional pseudocapacitance;[35] while surface acidic functional groups (carboxyl-type) play a negative role in supercapacitors, because they may cause substantial retardation of ion penetration into the pores during charging and discharging.[36] These groups can be selectively removed by controlled thermal treatment in inert gas. Therefore, RGO materials were thermally treated to 200, 400, 600, and 800 °C in order to enhance the energy storage properties.

The decomposition of oxygen-containing functional groups during TPD experiments in helium was monitored by mass spectrometric (MS) analysis of H_2O, CO_2, and CO evolved from RGO versus temperature up to 1000 °C. The heating rate (10 °C/min) in TPD measurements was the same as in TGA runs, which makes it possible to compare TGA weight loss data (Figure 2b) with the MS analysis of gas composition (Figure 2c) during heating in inert gas. Two significant losses occurred during TGA measurement, corresponding to release of physisorbed water (below 100 °C), and decomposition of labile oxygen-containing functional groups with release of carbon oxides and water (from 200 to ~600 °C). CO_2 evolution started before 200 °C, had the maximum rate at 350−400 °C, and continued with gradually diminishing intensity up to 1000 °C. In contrast, CO evolution increased with temperature but did not complete when the test has ended at 1000 °C. TPD decomposition of oxygen groups on activated carbons was well characterized. For CO_2 desorption, the peaks situated at 500−700, 350−450, and 220−300 °C correspond to the decomposition of lactones, carboxylic anhydrides and carboxylic acid groups, respectively.[37,38] The decomposition of quinones, carbonyl, phenols and anhydrides occurred at above

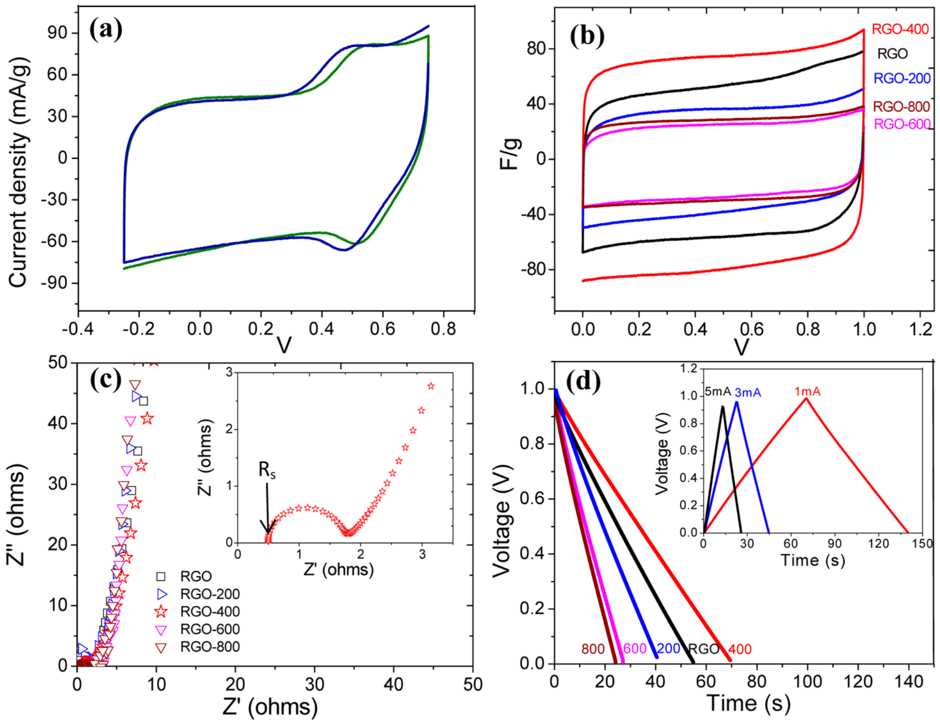

Figure 4. Supercapacitor performance of RGO thermally treated at various temperatures. (a) CV curves at 5 mV/s showing faradic processes overlapped over capacitive behavior for RGO-200; (b) stable CV curves for RGO treated at different temperatures showing rectangular shapes characteristic for capacitive behavior; (c) Nyquist plots for RGO treated at different temperatures. Inset shows a magnified plot for RGO-400 near origin and the corresponding semicircle which was used to extract the series resistance (R_s) value. (d) Galvanostatic discharge curves of RGO treated at various temperatures. Inset shows charge/discharge curves of RGO-400 at different constant current conditions.

800 °C, 700−770 °C, 600−700 °C, and 350−450 °C, respectively, resulting in the release of CO.[37,38] CO and CO_2 were generated from the decomposition of carboxylic and anhydrides. Either one CO_2 or two CO molecules can be produced based on the decomposition of one group semi-quinones.[38,39] CO_2 released above 770 °C is attributed to the disproportionation of CO into carbon dioxide and carbon (Boudouard reaction).[35,40]

Surface and pore-size characterization of the RGO after thermal treatments at various temperatures was performed by high-resolution N_2 (77.4 K) adsorption. Nitrogen isotherms, as shown in Figure 3a, are type II and present H3 type hysteresis, typical for disordered nonrigid aggregates of platelike solids forming slit-shaped pores.[41] Figure 3b displays the results of the total BET surface area and total pore volume calculated with the nonlocal density functional theory (NLDFT). The BET surface area increased gradually with the increase of treatment temperature up to 400 °C, from 311 m^2 g^{-1} for as-prepared materials to 429 m^2 g^{-1}, and then decreased to 375 m^2 g^{-1} at 800 °C. The ideal isolated graphene has a BET surface area of 2,620 m^2/g. The lower specific surface area of RGO is probably caused by the aggregation of RGO sheets during reduction process, leading to partial overlapping and coalescing. The total pore volume increases gradually with thermal treatment temperature, but decreases after 400 °C, which is consistent with specific surface area (Figure 3b). Figure 3c,d show the differential and cumulative distribution of pore volumes versus pore size. Micropores (pore sizes below 20 Å) are absent; all materials have bimodal mesopore distribution, a narrow range at 30−50 Å and a broader range between 150 and 400 Å range (Figure 3c).

Figure 4 shows the results of electrochemical characterization. Preliminary investigation of RGO materials using cyclic voltammetry did not detect any significant faradic (pseudocapacitive) behavior, with the exception of RGO (not thermally treated) and RGO-200. For the latter material a pair of pseudocapacitive peaks was occasionally observed at about 0.5 V (vs zero current potential, E_{oc}) which might be attributed to the reaction of electroactive surface groups, in particular the quinone − phenol redox reaction.[35,42] However, the pseudocapacitive peaks were not stable and disappeared after a few cycles. All subsequent results characterize stable charge/discharge behavior. Figure 4b shows reproducible CV cycles recorded in the two electrode configuration at a scan rate 5 mV/s in 5 M H_2SO_4. The shapes indicate an excellent capacitive behavior, low contact resistance, and no faradic processes. This character indicates that the electrode material is efficiently used for charge storage; the electrolyte has easy access to electrodes resulting in better ion diffusion due to the structure of thermally modified RGO. The increase in area of the CV curves indicates an enhancement of the specific capacitance. The total capacitance of the two-electrode assembly was calculated directly from the current−potential curves as $C_t = I(d\Delta E/dt)^{-1}$, where I is the current and E is the potential difference. The material-specific capacitance was calculated as $C_g = 4C_t/m$ where m is the total weight of activated carbon. The factor 4 in this formula accounts for series capacitances and for double weight of carbon on the two electrodes.[43]

Nyquist plots with frequency range from 1 MHz to 10 mHz are shown in Figure 4c. A sharp increase at low frequencies indicates the capacitive behavior of the electrode. For an ideal double-layer capacitor, the impedance plot should be a vertical

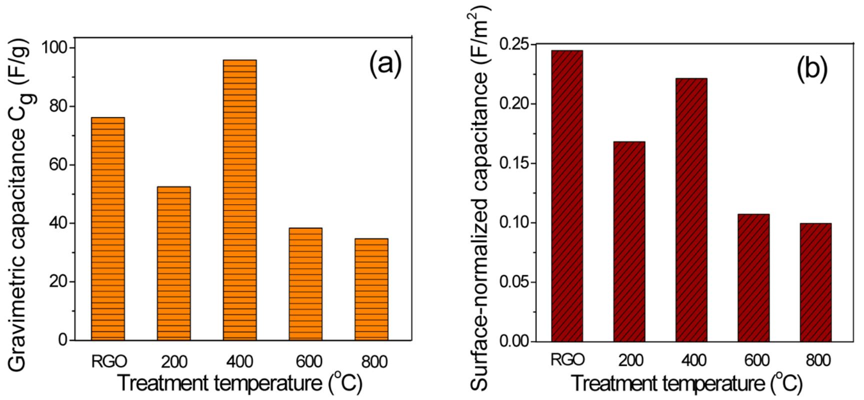

Figure 5. Plot of gravimetric capacitance of the graphene-based supercapacitors and their specific capacitance normalized by BET Surface areas.

line, parallel to the imaginary axis. The plots in Figure 4c feature almost vertical curves, indicating the excellent capacitive behavior of the cells. A magnified Nyquist plot for RGO-400 in the inset of Figure 4c is typical for capacitive behavior at low frequencies coupled with diffusional impedance caused by slower migration of electrolyte ions in pores at high frequencies.[44] The electrode series resistance (ESR) values determined from the first intersection of the semicircle with the real axis, R_s were all in the range of 0.50−0.55 ohm. Figure 4d shows the galvanostatic discharge curves of graphene materials treated at various temperatures in the potential range 0−1 V at constant current density of 0.3 A/g. The galvanostatic charge/discharge curves of RGO-400 are shown in the inset of Figure 4b. The plots are linear and symmetrical, showing capacitive behavior and no faradic processes.

Figure 5 shows the gravimetric specific capacitance C_g and surface-normalized specific capacitance C_s as a function of the treatment temperature. The highest specific capacitance was obtained for RGO-400 (C_g = 96 F/g). The enhancement of the specific capacitance at 400 °C can be partially attributed to the development of BET surface area (Figure 3b). Because all materials investigated here have relatively low BET surface area, the corresponding gravimetric capacitance is still below the level characteristic for high surface area carbons (which can reach up to 150−200 F/g in aqueous H_2SO_4 solutions[45]).To allow comparison with other material-specific reports[46] and ascertain the effect of treatment temperature, irrespective of surface area, Figure 5 also shows area-specific capacitance values C_s normalized to the BET surface area. Increasing the treatment temperature appeared to have in general a detrimental effect on the weight-normalized capacitance, C_g; however, the surface-normalized capacitance C_s obviously rebounded at about 400 °C and reached 0.22 F/m^2. This value is higher than the range (0.07−0.13 F/m^2) reported for commercial activated carbon and many other high surface area carbons (including carbide-derived carbons and carbon nanotubes) in aqueous H_2SO_4 electrolyte solutions.[46,47] This high value of C_s is 1 order of magnitude higher than the double-layer capacitance of graphite basal planes (0.03 F/m^2) and between half to one-third of that estimated for graphite edge planes (0.50−0.70 F/m^2),[47] showing a high contribution of edge sites to the specific capacitance of RGO-400. At this temperature, carboxyl groups decompose to CO_2 and H_2O, whereas quinone-type functional groups are still stable (Figure 2c). We assume therefore that the increase in surface-normalized capacitance at 400 °C is caused by the removal of most of carboxyl-type groups which are known to hinder ion penetration into the pores.[36] At higher temperatures (600 and 800 °C) quinone groups start decomposing, releasing either CO_2 or CO (Figure 2c). This process causes further collapse of BET surface area and porosity (Figure 3b) and hence results in lower capacitances, both C_g and C_s.

The dynamic Ragone plot in Figure 6a shows the variation of power density (PD) versus energy density (ED) during galvanostatic discharge at I = 1 mA for the original RGO and four temperature-treated materials. During galvanostatic discharge, these electrode-specific values decline in a manner dependent on the rate of discharge as the capacitor's potential

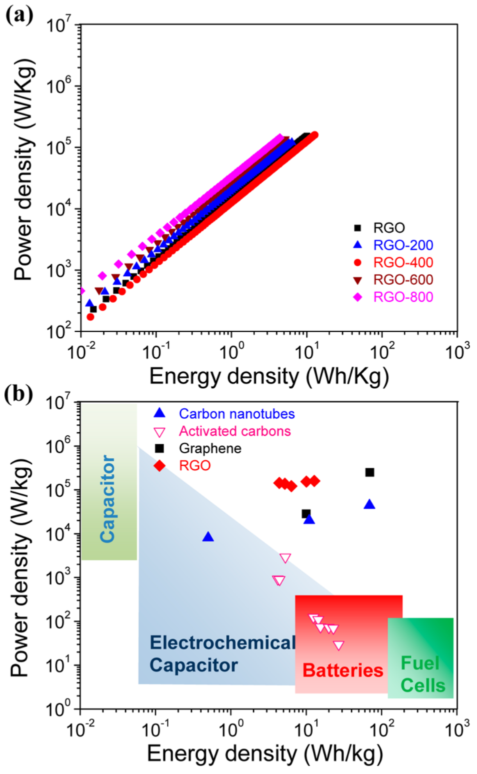

Figure 6. (a) Dynamic Ragone plots showing power density versus available energy density during constant current (1 mA) discharge of RGO electrodes in 5 M H_2SO_4. (b) Ragone plot showing maximum power and energy density of RGO materials (calculated for ΔE = 1 V) in comparison with reported graphene materials,[18,20] carbon nanotubes,[14,48,49] activated carbons[3,50] as supercapacitors. The ranges reported for common classes of energy storage devices are also shown.[41,47]

changes when energy is withdrawn from the material.[49] Such plots depict a fundamental property of electrochemical capacitors, namely the continuous decline of PD and available ED with decreasing state of charge. The values shown in Figure 6a were calculated using ED = 0.5 $CV^2 = 0.5\ C_g\ [V(t) - IR_s]^2$, where R_s is the ESR estimated from the Nyquist plots at high frequencies and I is the current; and PD = $V(t)^2/4mR_s$ where m is the mass of the two electrodes.[18,20] The corresponding device-specific characteristics depend strongly on the configuration and materials used for building full size capacitors.[51] We estimated their values using the highest values for PD and ED measured for each (fully charged) cell assembled with modified RGO materials. The values plotted in Figure 6b are compared with those reported for activated carbon, carbon nanotubes, and other graphene materials in supercapacitors, and with the performance limits characteristic for other power storage devices.[47,52] The experimental curves of PD versus ED in 5 M H_2SO_4 show the superior performance of RGO treated at 400 °C.With a cell voltage of 1.0 V, ESR of 0.5 ohm and mass of 0.003 g, the maximum power density of ~160 kW/kg for RGO-400 was thus obtained. This power density is higher than the values reported for carbon nanotubes[14,48,49] and two orders higher than the values for commercial carbon supercapacitors with power density values of 3 to 8 kW/kg.[3] With the capacitance value of 96 F/g, a maximum energy density of 12.8 Wh/kg is obtained for RGO-400, which is higher than some reported energy density for the available CNT-based devices[53] and comparable with high surface area carbons.

CONCLUSION

Graphene materials prepared by a modified Hammers method and hydrazine reduction were characterized at various stages during synthesis. RGO forms a continuous network of crumpled sheets, which consist of large amounts of few-layer and single-layer graphenes, still rich in oxygen. Thermal treatment at 400 °C is beneficial for surface area and specific capacitance, but higher treatment temperatures had a negative effect on these properties. The best performance was measured for RGO-400, namely material-specific capacitance of 96 F/g; area-normalized capacitance up to 0.22 F/m^2 (higher than most high surface area carbon materials), and projected energy density (12.8 Wh/kg) and power density (160 kW/kg). The results demonstrate that thermal treatment of RGO at selected conditions is a convenient and efficient method for improving specific capacitance, energy, and power density.

AUTHOR INFORMATION

Corresponding Author

*Fax: +1 865 576 8424. E-mail: contescuci@ornl.gov.

Notes

The authors declare no competing financial interest.

ACKNOWLEDGMENTS

This research was supported by the Laboratory Director Research and Development Program of Oak Ridge National Laboratory, managed by U.T. Battelle LLC for the US Department of Energy. SEM and X-ray diffraction were performed at the Shared Research Equipment (SHaRE) user facility, and Raman and AFM characterization were performed at the Center for Nanophase Materials Science (CNMS), both of which are supported at Oak Ridge National Laboratory by the Division of Scientific User Facilities, U.S. Department of Energy. The authors acknowledge Mr. Jimmy Zahra for the kind assistance during galvanostatic charge-discharge, CV, and EIS measurements. HZ acknowledges support from ORISE/ORNL postdoctoral program.

REFERENCES

(1) Miller, J. R.; Simon, P. *Science* **2008**, *321*, 651.

(2) Simon, P.; Gogotsi, Y. *Nat. Mater.* **2008**, *7*, 845.

(3) Burke, A. *Electrochim. Acta* **2007**, *53*, 1083.

(4) Zhu, Y. W.; Murali, S.; Stoller, M. D.; Ganesh, K. J.; Cai, W. W.; Ferreira, P. J.; Pirkle, A.; Wallace, R. M.; Cychosz, K. A.; Thommes, M.; Su, D.; Stach, E. A.; Ruoff, R. S. *Science* **2011**, *332*, 1537.

(5) Brezesinski, T.; Wang, J.; Tolbert, S. H.; Dunn, B. *Nat. Mater.* **2010**, *9*, 146.

(6) Fernandez, J. A.; Arulepp, M.; Leis, J.; Stoeckli, F.; Centeno, T. A. *Electrochim. Acta* **2008**, *53*, 7111−7116.

(7) Subramanian, V.; Luo, C.; Stephan, A. M.; Nahm, K. S.; Thomas, S.; Wei, B. *J. Phys. Chem. C* **2007**, *111* (20), 7527.

(8) Kim, H.; Popov, B. N. *J. Electrochem. Soc.* **2003**, *150* (3), D56.

(9) Roberts, M. E.; Wheeler, D. R.; McKenzie, B. B.; Bunker, B. C. *J. Materials. Chem.* **2009**, *19* (38), 6977.

(10) Rudge, A.; Davey, J.; Raistrick, I.; Gottesfeld, S.; Ferraris, J. P. *J. Power Sources* **1994**, *47*, 89.

(11) Chmiola, J.; Yushin, G.; Gogotsi, Y.; Portet, C.; Simon, P.; Taberna, P. L. *Science* **2006**, *313*, 1760.

(12) Huang, J.; Sumpter, B. G.; Meunier, V. *Angew. Chem., Int. Ed.* **2008**, *47*, 520.

(13) Zhang, Y.; Feng, H.; Wu, X.; Wang, L.; Zhang, A.; Xia, T.; Dong, H.; Li, Z.; Zhang, L. *Int. J. Hydrogen Energy* **2009**, *34*, 4889.

(14) Futaba, D. N.; Hata, K.; Yamada, T.; Hiraoka, T.; Hayamizu, Y.; Kakudate, Y.; Tanaike, O.; Hatori, H.; Yumura, M.; Iijima, S. *Nat. Mater.* **2006**, *5*, 987.

(15) Geim, A. K.; Novoselov, K. S. *Nature* **2007**, *6*, 183.

(16) Park, S.; Rouff, R. S. *Nature* **2009**, *4*, 217.

(17) Stoller, M. D.; Park, S.; Zhu, Y.; An, J.; Rouff, R. S. *Nano Lett.* **2008**, *8*, 3498.

(18) Zhu, Y. W.; Murali, S.; Stoller, M. D.; Ganesh, K. J.; Cai, W. W.; Ferreira, P. J.; Pirkle, A.; Wallace, R. M.; Cychosz, K. A.; Thommes, M.; Su, D.; Stach, E. A.; Ruoff, R. S. *Science* **2011**, *332*, 1537.

(19) Stankovich, S.; Dikin, D. A.; Piner, R. D.; Kohlhaas, K. A.; Kleinhammes, A.; Jia, Y.; Wu, Y.; Nguyen, S. T.; Ruoff, R. S. *Carbon* **2007**, *45*, 1558.

(20) Wang, Y.; Shi, Z.; Huang, Y.; Ma, Y.; Wang, C.; Chen, M.; Chen, Y. *J. Phys. Chem. C* **2009**, *113*, 13103.

(21) Zhao, N; Liu, P; Jiang, Y; Pan, D; Tao, H; Song, J; Fang, T; Xu, W *J. Power Sources* **2012**, *198*, 423.

(22) Hummers, W. S.; Offeman, R. E. *J. Am. Chem. Soc.* **1958**, *80*, 1339.

(23) Saxena, S.; Tyson, T. A.; Negusse, E. *J. Phys. Chem. Lett.* **2010**, *1*, 3433.

(24) Yuge, R.; Zhang, M.; Tomonari, M.; Yoshitake, T.; Iijima, S.; Yudasaka, M. *ACS-Nano* **2008**, *2*, 1865.

(25) Brunauer, S; Emmett, P. H.; Teller, E. *J. Am. Chem. Soc.* **1938**, *60*, 309.

(26) Lastoskie, C. M.; Gubbins, K.; Quirke, N. *Langmuir* **1993**, *9*, 2693.

(27) Meyer, J. C.; Geim, A. K.; Katsnelson, M. I.; Novoseleov, K. S.; Booth, T. J.; Roth, S. *Nature* **2007**, *446*, 60.

(28) Yan, J.; Wei, T.; Shao, B.; Ma, F.; Fan, Z.; Zhang, M.; Zheng, C.; Shang, Y.; Qian, W.; Wei, F. *Carbon* **2010**, *48*, 1731.

(29) Hontoria-Lucas, C.; Lopez-Peinado, A. J.; Lopez-Gonzalez, J. D. D.; Rojas-Cervantes, M. L.; Martin-Aranda, R. M. *Carbon* **1995**, *33* (11), 1585.

(30) Tuinstra, F.; Koenig, J. L. *J. Chem. Phys.* **1970**, *53* (3), 1126.

(31) Montes-Moran, M. A.; Suarez, D.; Menendez, J. A.; Fuente, E. *Carbon* **2004**, *42*, 1219.

(32) Leon, C. A. L. Y.; Radovic, L. R. *Chem. Phys. Carbon* **1994**, *24*, 213.

(33) Szabo, T.; Tombacz, E.; Illes, E.; Dekany, I. *Carbon* **2006**, *44*, 537.
(34) Li, L.; Liu, E.; Li, J.; Yang, Y.; Shen, H.; Huang, Z.; Xiang, X.; Li, W. *J. Power Sources* **2010**, *195* (5), 1516.
(35) Andreas, H . A.; Conway, B. E. *Electrochim. Acta* **2006**, *51*, 6510.
(36) Kim, C. H.; Pyum, S. I.; Shin, H. C. *J. Electrochem. Soc.* **2002**, *149*, A93.
(37) Zielke, U.; Huttinger, K. J.; Hoffman, W. P. *Carbon* **1996**, *34*, 983.
(38) Almarri, M.; Ma, X.; Song, C. *Energy Fuels* **2009**, *23*, 3940.
(39) Boehm, H. P. *Carbon* **2002**, *40*, 145.
(40) Hall, P. J.; Calo, J. M. *Energy Fuels* **1989**, *3*, 370.
(41) Lowell, S.; Shields, J. E.; Thomas, M. A.; Thommes, M. *Characterizaiton of Porous Solids and Powders: Surface Area, Pore Size and Density*; Kluwer Academic:Dordrecht, The Netherlands, 2010; pp 43−45.
(42) Frackowiak, E.; Beguin, F. *Carbon* **2001**, *39*, 937.
(43) Janes, A.; Kurig, H.; Lust, E. *Carbon* **2007**, *45*, 1226.
(44) Conway, B. E. *Electrochemical Supercapacitors*; Kluwer Academic/Plenum Publishers: Dordrecht, The Netherlands, 1999; pp 519−555.
(45) Frackowiak, E. *J. Braz. Chem. Soc.* **2006**, *17* (6), 1074.
(46) Chmiola, J.; Yushin, G.; Dash, R. K.; Hoffman, E. N.; Fisher, J. E.; Barsoum, M. W.; Gogotsi, Y. *Electrochem. Solid-State Lett.* **2005**, *8* (7), A357.
(47) Pandolfo, A. G.; Hollenkamp, A. F. *J. Power Sources* **2006**, *157*, 11.
(48) Du, C.; Pan, N. *Nanotechnology* **2006**, *17*, 5314.
(49) Niu, J.; Pell, W. G.; Conway, E. *J. Power Sources* **2006**, *156*, 725.
(50) Wang, Y.; Wang, C.; Guo, C.; Shi, Z. J. *J. Phys. Chem. Solids* **2008**, *69*, 16.
(51) Stoller, M. D.; Ruoff, R. S. *Energy Environ. Sci.* **2010**, *3*, 1294.
(52) Basic Research Needs for Electrochemical Energy Storage, Office of Basic Energy Science, Department of Energy, July 2007 (http://www.sc.doe.gov/bes/reports/files/EES_rpt.pdf)
(53) Mohana, R. A. L.; Shaijumon, M. M.; Gowda, S. R.; Ajayan, P. M. *J. Phys. Chem. C* **2010**, *114*, 658.